Performance of alloy 600 in flowing commercial Cl salt at 600°-750°C

Bruce A. Pint[1, a)] J. Matthew Kurley[1, b)] and Dino Sulejmanovic[1, c)]

[1]*Corrosion Science and Technology Group, Materials Science and Technology Division, Oak Ridge National Laboratory, 1 Bethel Valley Rd., Oak Ridge, TN 37831 USA*

a) Corresponding author: pintba@ornl.gov
b)kurleyjm@ornl.gov
c)sulejmanovid@ornl.gov

Abstract. For the next generation of concentrating solar power (CSP) plants, K-Mg-Na chloride salts are being explored as a potential higher temperature thermal storage medium. However, there are concerns about compatibility of structural alloys with the salt. To move beyond simple static pot compatibility experiments while a pumped salt loop is being constructed, thermal convection loops were constructed from ~16wt.%Cr Ni-based alloy 600 and operated for 100-1000 h with peak temperatures of 700° and 750°C. These experiments indicated that alloy 600 was compatible up to 700°C with purified (i.e. low O^{2-}) or dried (low H_2O) industrial-sourced Mg-K-Na chloride salt with <10 µm/yr loss. Mass transfer was observed from the hot leg to the cold leg in each experiment and more surface deposits were observed with the dried salt. Post-exposure room temperature tensile tests showed minimal degradation of alloy 600 under these conditions.

INTRODUCTION

For the next generation of higher efficiency concentrated solar power (CSP), a supercritical CO_2 (sCO_2) power block [1] operating at >700°C paired with chloride salt thermal storage [2] is envisaged to yield >50% electrical efficiency. However, many recent reports in the literature suggest that chloride salts are highly corrosive to structural alloys [3,4] but do not clearly describe how the salt was handled, dried and/or purified prior to the corrosion experiments and used isothermal experiments which do not study mass transfer in a flowing system with a temperature gradient. Historically at Oak Ridge National Laboratory (ORNL), reasonably good compatibility was achieved with purified halide salts flowing in a temperature gradient [5,6] so this project used similar strategies to illustrate that dried or purified industrial-sourced commercial K-Mg-Na chloride salt showed reasonable compatibility with Ni-based alloy 600 (Table 1) at salt temperatures of 600°-750°C.

PROCEDURE

The established ORNL methodology for evaluating compatibility [6-11] is to begin testing using sealed capsules and those results are reported elsewhere including more details on salt preparation and the experimental procedures [10,11]. Flowing experiments were conducted using harp-shaped (~0.75 m tall by 0.5 m wide) thermal convection

TABLE 1. Alloy chemical composition in weight % measured using inductively coupled plasma and combustion analyses.

Alloy	Ni	Cr	Fe	Al	W	Mo	Ti	Mn	Si	S(ppm)	Other
600T	75.5	15.3	9.4	0.2	0.01	0.01	0.15	0.60	0.16	<3	0.05C
600S	77.1	14.4	7.3	0.2	<0.01	<0.01	0.20	0.37	0.30	4	0.08C

loops (TCL), which have been described in detail elsewhere [6,9-11]. The TCL was made from alloy 600 tubing (25 mm OD x 1.2mm wall, 600T in Table 1) and the specimen chains in the vertical hot and cold legs consisted of 20 specimens each including small dogbone tensile specimens (25mm long with a 1.5 x 0.76 mm gage, designated SS-3) and coupons (1.8 x 19 x 25 mm) all polished to a 600 grit finish (600S in Table 1). Experiments #2 and #3 also contained C276 specimens [11]. For TCL experiments #1 and #2, commercial 43:53:4 K:Mg:Na Cl salt (As-rec. #1 in Table 2) was purified using NH_4Cl and CCl_4 in two steps [10,12] and 0.04%Mg was added. For the third experiment, commercial 40:40:20 K:Mg:Na Cl salt (mixture of As-rec. #2 and Halite in Table 2) was dried during heating to 670°C [11] and both 0.05%Mg was added to the salt and a Mg coupon was hung at the bottom of the cold leg specimen chain. Three resistively heated furnaces heated the hot leg and temperatures were monitored using 6 type K thermocouples in thermowells in the hot and cold legs. The loop temperature was controlled at the top of the hot leg to 700±1°C or 750±2°C. The 700°C TCLs were for 1000 h, the 750°C TCL only operated for ~110 h before a furnace failed (not related to salt compatibility). The salt flow rate was ~2.4 cm/s in each 1000 h experiment and was not measured in experiment #2. In each case, the specimens were cleaned after exposure using deionized water at 40°C. Before and after exposure, the specimens were weighed using a Mettler Toledo model XP205 balance with an accuracy of ~±0.04 mg. The specimens were then sectioned and mounted in epoxy and polished for characterization using light microscopy and secondary electron microscopy (SEM) equipped with energy dispersive x-ray spectroscopy (EDS). Glow discharge optical emission spectroscopy (GDOES) also was used to measure the composition of the reaction products. Depth profiles were acquired by sputtering the surfaces with an electric field-induced glow discharge plasma using low-pressure argon at 50W with measurements made every 0.1 s with an anode diameter of 4 mm which defined the size of the region measured. Room temperature tensile tests were conducted with a strain rate of $\sim 10^{-3}\ s^{-1}$.

RESULTS & DISCUSSION

1st and 2nd TCL Experiments in Purified Commercial Salt

Figure 1 shows the mass change data from the alloy 600 specimens exposed to purified salt with 0.04%Mg as a function of the estimated exposure temperature of the specimens in the hot leg (HL) and cold leg (CL). In the 1st TCL experiment with a peak temperature of 700°C and a 1000 h exposure, the maximum mass loss corresponds to a ~9 μm/year loss [10]. The general behavior of mass loss in the hot leg and mass gain in the cold leg suggests mass transfer.

Consistent with this mechanism, Figures 2b and 2c show the surface pitting observed at the top of the hot leg at estimated temperatures of 690° and 681°C, respectively. The first specimen in the chain near the corner of the loop did not show pitting, Figure 2a. At the bottom of the cold leg, deposits were evident on the surface, Figures 2i-2l. Figure 3 shows SEM/EDX maps of the 690°C HL specimen where some Cr depletion was observed but only to depth of ~10 μm. The depletion was from ~14wt.%Cr (Table 1) to ~10%Cr. There appeared to be C enriched at the specimen surface, Figure 3h, but C is difficult to detect and quantify using EDX. The alloy contained Ti nitride precipitates, Figures 3e and 3j, and no Mg enrichment at the surface was observed. Figure 4a shows an EDX line profile from the specimen exposed to salt at ~589°C at the bottom of the cold leg. Based on the Cr depletion in the hot leg, Cr enrichment might be expected. Instead, the surface was slightly Fe enriched.

TABLE 2. Chemical composition of the industrial-sourced salt determined by ICP for each of the salt variations and acid-base titration of the O^{2-} content of the dried salt.

	K (%)	Mg (%)	Na (%)	Ca (%)	Br (%)	S (ppm)	Ni (ppm)	Fe (ppm)	Cr (ppm)	Mn (ppm)	W (ppm)	Al (ppm)	O^{2-} (μmol/kg)
As-rec. #1	19.7	12.8	1.55	n.d.	0.61	n.d.	n.d.	4.7	n.d.	3.4	n.d.	n.d.	
Purified	20.1	12.9	1.62	n.d.	n.d.	n.d.	n.d.	1.7	n.d.	1.2	n.d.	n.d.	197
As-rec. #2	20.6	12.2	4.8	0.09	0.14	79	0.3	67	0.2	4	0	2	
Halite	7.9	0.02	31.9	0.26	0.01	6618	0.1	82	0.1	5	0	104	
Dried	18.5	11.2	7.1	0.12	0.14	344	0.4	90	0.04	5	0	4	>20,000
After #3	19.2	11.5	6.8	0.13	0.14	15	**56**	94	**229**	37	44	1	

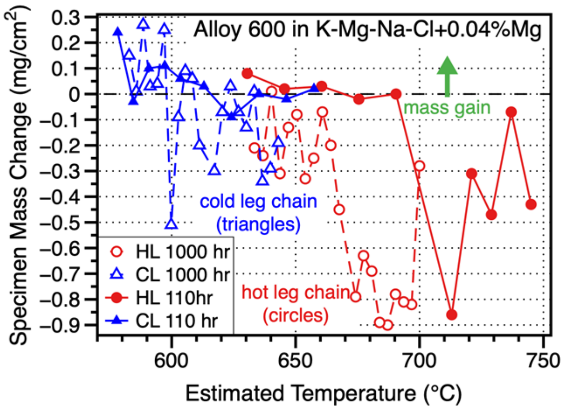

FIGURE 1. Specimen mass change as a function of estimated exposure temperature in flowing, purified, commercial Cl salt. The open symbols show the 1st experiment that ran for 1000 h and the closed symbols show the 2nd experiment that ran for 110 h.

With the Mg addition to the salt, there was a concern that Mg would be deposited on the specimens, as has been seen in capsule experiments [10,11]. Figure 4b shows the GDOES profiles from four coupons and an unexposed specimen. Since there is no Mg in alloy 600, there was no standard for comparison. The intensity from a pure Mg specimen was 222 suggesting the largest signal from the specimen exposed at 589°C in the CL had <1% Mg detected.

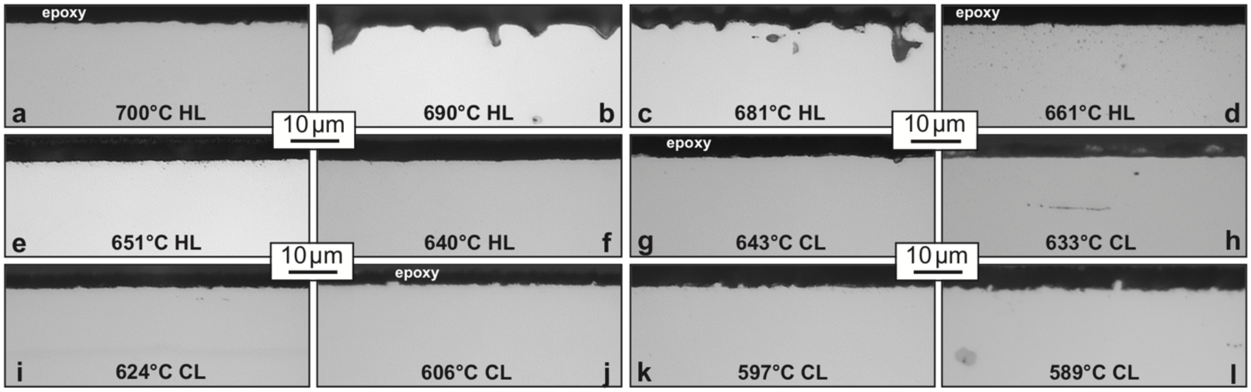

FIGURE 2. Light microscopy of polished cross sections of alloy 600 specimens exposed for 1000 h in flowing, purified commercial Cl salt, the estimated exposure temperature in the hot leg (HL) and cold leg (CL) are shown in each image.

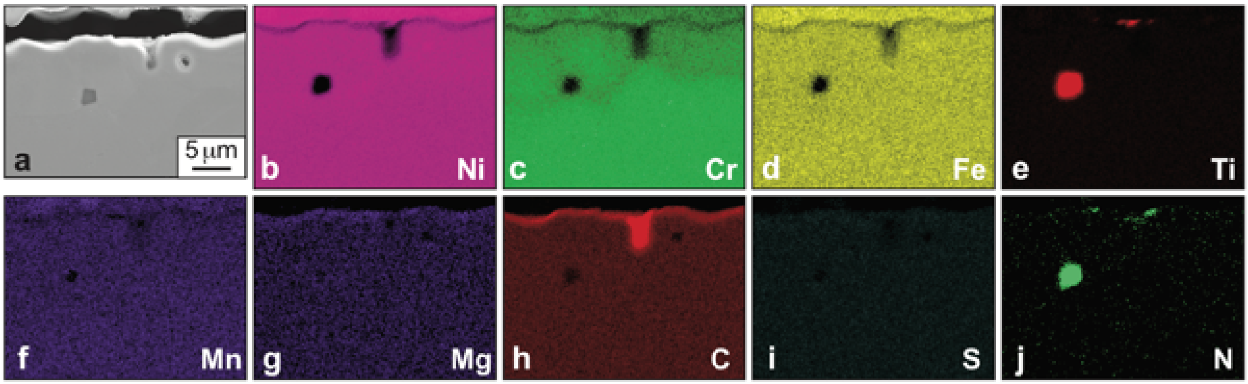

FIGURE 3. Polished cross-section of alloy 600 specimen exposed at ~690°C for 1000 h in flowing, purified commercial Cl salt (a) SEM secondary electron image and (b-j) EDX maps of the same region.

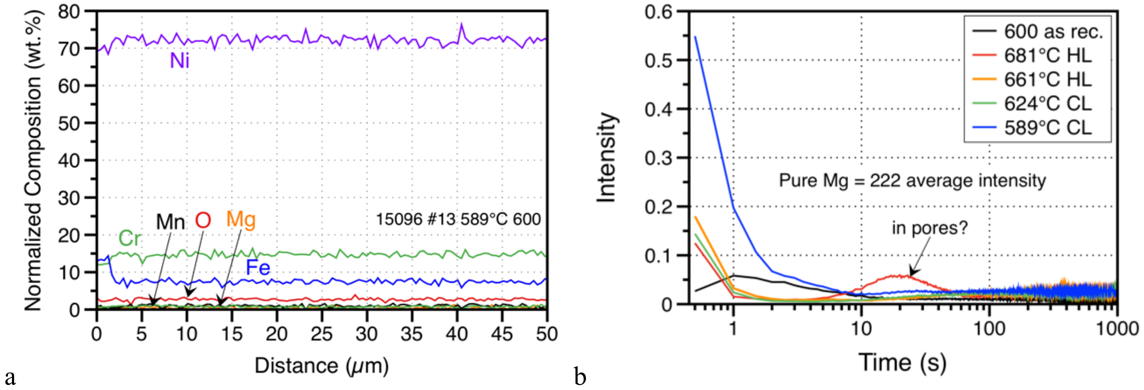

FIGURE 4. (a) EDX line profile from alloy 600 specimen exposed for 1000 h at 589°C in the cold leg (CL) of TCL #1 and (b) GDOES Mg depth profiles of alloy 600 specimens after 1000 h exposures in flowing purified salt + 0.04%Mg identified by their exposure temperature. An unexposed (as received) alloy 600 specimen is shown for reference.

Figure 1 also shows the mass change data for the alloy 600 specimens from the 2nd TCL experiment where the same alloy 600 loop was used with a new set of specimens and the peak temperature was increased to 750°C. Due to a furnace failure during a holiday weekend, the experiment only ran for ~110h at temperature. Efforts to remelt the salt in the loop were unsuccessful and the specimens were removed and cleaned. The mass changes were similar for the 2nd TCL experiment due to the shorter time at higher temperature suggesting that more mass change would have been observed if the experiment ran for 1000 h. Figure 5 shows polished cross-sections of alloy 600 coupon specimens after exposure. Similar to the 1st experiment, pitting was observed at the top of the hot leg at 745° and 721°C and deposits were observed in the cold leg at 657°-578°C, Figure 5. At this time, it was decided to switch salts for future work and no further characterization of these specimens was conducted.

3rd TCL Experiment in Dried Commercial Salt

A new salt composition was selected for the 3rd TCL experiment with a lower melting point achieved by increasing the Na content, Table 2. Also, a simpler salt preparation procedure was selected more amenable to the large salt quantities required for CSP. However, this procedure dried the salt but left an unmeasurably large O^{2-} content in the salt, orders of magnitude higher than the purified salt, Table 2.

Figure 6 compares the mass change with pure salt (Figure 1) to the TCL experiment using the dried salt with a 0.05%Mg addition. The dried salt TCL experiment also contained a Mg specimen at the bottom of the cold leg to control the salt redox potential. Slightly higher mass gains were observed in the dried salt in the hot and cold legs but the observed attack was minimal, suggesting the drying procedure was sufficient for improving compatibility with alloy 600 in this temperature range.

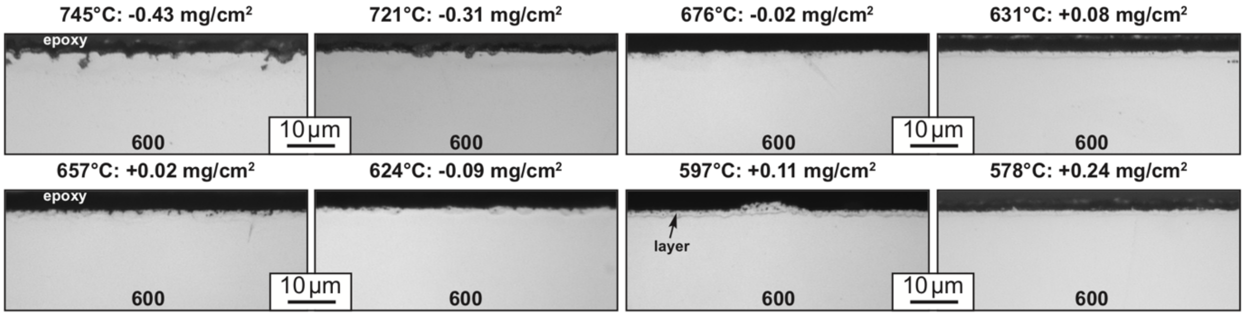

FIGURE 5. Light microscopy of polished cross sections of alloy 600 specimens exposed for 110 h in flowing, purified commercial Cl salt, the estimated exposure temperature in the hot leg (top row) and cold leg (bottom row) are shown.

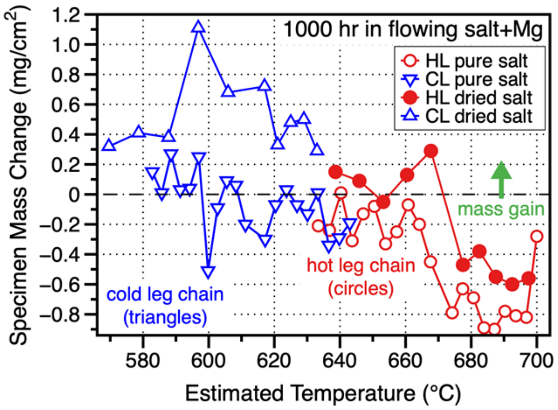

FIGURE 6. Specimen mass change as a function of estimated exposure temperature after 1000 h exposures in two different flowing commercial Cl salts. The open symbols show the 1st experiment in purified salt and the closed symbols show the 3rd experiment in dried salt.

Figure 7 shows polished cross-sections from the alloy 600 coupon specimens. Compared to similar images in Figure 2, there appear to be more deposits but a similar depth of affected metal. Similar to the 1st TCL experiment, Cr depletion was observed in the hot leg specimens that lost mass. From the cold leg, Figure 8 shows EDX maps from the alloy 600 specimen exposed at ~621°C. A depth of ~5 μm was depleted in Cr and concurrently enriched in Fe, Figures 8c and 8f, respectively. The surface layer was enriched in Mg, C, O and Al, Figures 8c, 8d, 8g and 8h. This is quite different from the TCL #1 cold leg specimen shown in Figure 4a. A similar EDX line profile from TCL #3 is shown in Figure 9a for a specimen exposed at ~597°C. For this specimen, a significant Mg surface enrichment was observed.

Figure 9b attempts to quantify the thickness of the outer layer and the depth of internal attack as a function of the estimated exposure temperature. Box and whiskers are used with the box defined as the 25 and 75% values of ~30 measurements in three representative images and the whiskers showing the minimum and maximum values measured. The median values are noted and the open boxes are from hot leg specimens and shaded boxes from cold leg specimens. Not all of the specimens showed measurable features. The 597°C specimen in Figure 8 is highlighted as one where an oxide layer was clearly formed. While some internal attack and deposition was observed, it is clear that all of the median values are <10 μm. Thus in all three TCL experiments, the observed attack was minimal and not consistent with the recent Cl salt literature. The addition of Mg to the salt was likely beneficial but 0.04-0.05%Mg was added in each of these experiment so it is not possible to determine its effect.

Finally, Figures 10 and 11 summarize the post-exposure room temperature tensile properties. The shaded areas in both cases show the as-received tensile properties and the open symbols show the result after the 1st TCL experiment for reference where only minimal changes were observed after exposure to flowing salt. Thermal annealing for 1000 h at 600°, 650°, 700° and 750°C also did not significantly change these values. In Figure 10, the closed symbols show the results from the 2nd TCL experiment. Slightly larger drops in the 0.2% yield stress (YS) and ductility were observed but the lowest value observed was still ~40%. A value below 10% would be cause for concern.

In Figure 11, the 3rd TCL specimen results are shown as larger open symbols. Only minor changes in YS and ultimate tensile stress were measured, Figure 11a. However, larger drops in ductility were observed compared to TCL #1 but similar to the values in Figure 10b. Overall, it appears that the impact of salt exposure to room temperature mechanical properties of alloy 600 is minimal.

Considerable work remains to be done to understand the effect of salt impurities and additives as well as higher temperatures. However, these results provide some confidence that there is an operating window for dried chloride salt as a thermal storage medium for CSP.

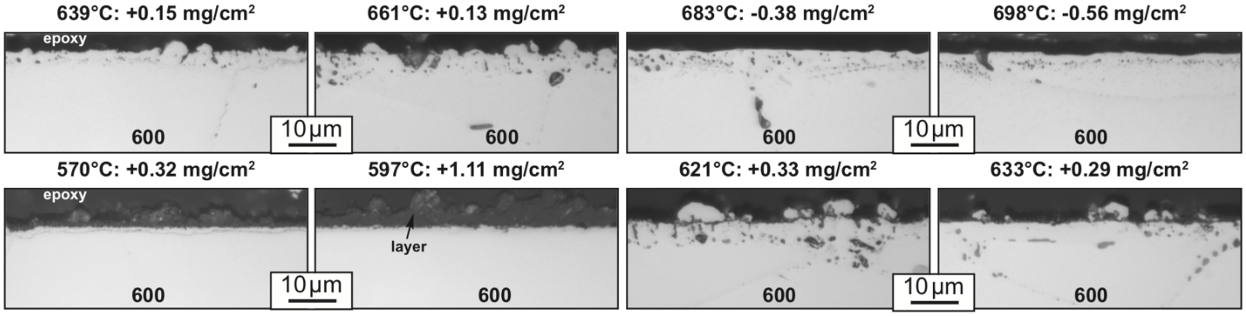

FIGURE 7. Light microscopy of polished cross sections of alloy 600 specimens exposed for 1000 h in flowing, dried, industrial-sourced K-Mg-Na Cl salt, the estimated exposure temperature in the hot leg (top row) and cold leg (bottom row) are shown.

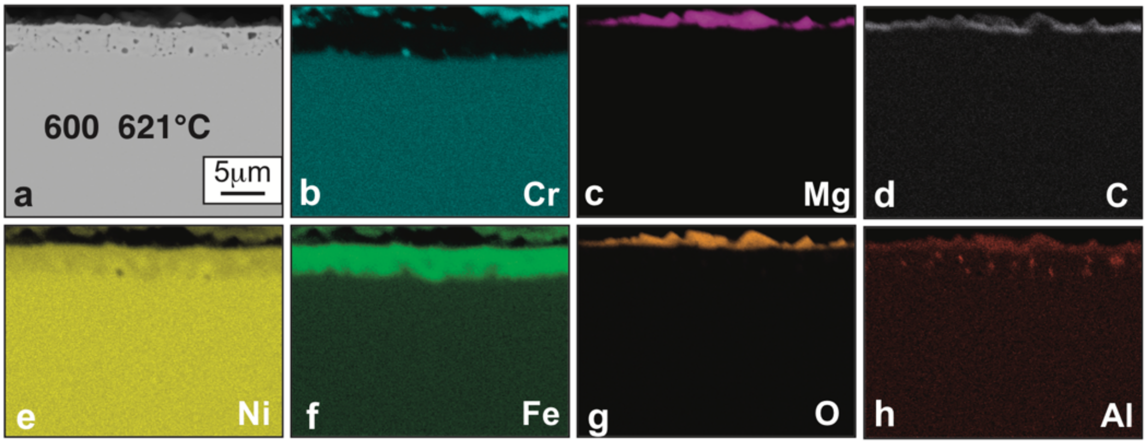

FIGURE 8. Polished cross-section of alloy 600 specimen exposed for 1000 h in flowing, dried commercial Cl salt at 621°C in the cold leg (a) SEM secondary electron image and (b-h) EDX maps of the same region.

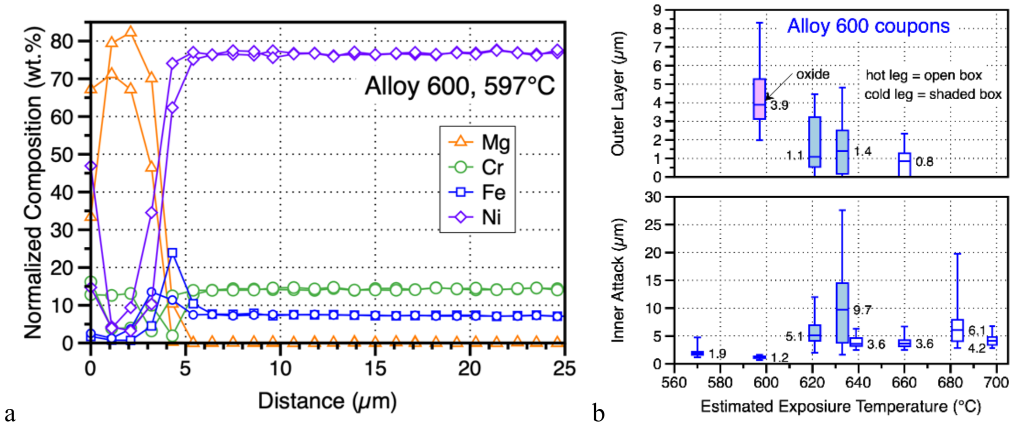

FIGURE 9. (a) box and whisker plots of the observed depth of attack and outer layer measured as a function of location in TCL #3, the median values are shown and (b) EDX line profiles from the alloy 600 specimen exposed in the cold leg at ~597°C

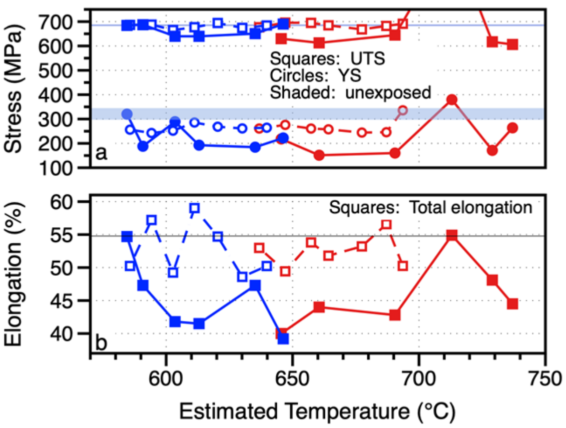

FIGURE 10. Room temperature mechanical properties (10^{-3} s^{-1} strain rate) of alloy 600 after exposure to flowing purified industrial-sourced salt as a function of estimated exposure temperature comparing the 1st TCL experiment (open symbols) and 2nd TCL experiment (closed symbols). (a) 0.2% yield stress (YS) and ultimate tensile stress (UTS) and (b) total elongation. The shaded region shows the range of values for unexposed specimens. Minimal degradation in properties was observed.

SUMMARY

These TCL experiments with flowing, industrial-sourced K-Mg-Na chloride salt demonstrated that there are potential materials solutions for the next generation of CSP plants with ≥50% efficiency and operation at ≥700°C with chloride salt thermal storage. Small mass changes and limited depth of attack were observed for both purified and dried salt with a peak temperature of 700°C. The 110 h exposure with a peak temperature of 750°C suggests that increasing the temperature will significantly increase the reaction rate but further testing is needed to determine the maximum operating temperature for this combination of materials.

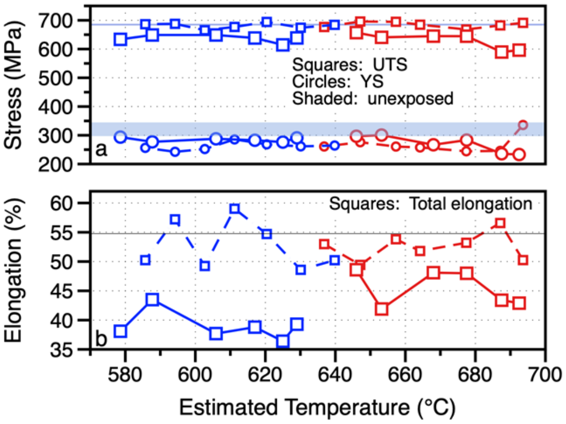

FIGURE 11. Room temperature mechanical properties (10^{-3} s^{-1} strain rate) of alloy 600 after exposure to flowing industrial-sourced salt as a function of estimated exposure temperature comparing the 1st TCL experiment (open symbols) and 3rd TCL experiment (closed symbols). (a) 0.2% yield stress (YS) and ultimate tensile stress (UTS) and (b) total elongation. The shaded region shows the range of values for unexposed specimens. Minimal degradation in properties was observed.

ACKNOWLEDGMENTS

The authors would like to thank A. Willoughby, M. Stephens, T. Lowe, T. Jordan, V. Cox, M. Lance and R. Mayes at ORNL for assistance with the experimental work and J. R. Keiser and R. Pillai for comments on the manuscript. This research was funded by the U.S. Department of Energy's Office of Energy Efficiency and Renewable Energy, Solar Energy Technology Program: CSP award number 33873. The input of L. Irwin as the technical project monitor is appreciated. This manuscript has been authored by UT-Battelle, LLC under Contract No. DE-AC05-00OR22725 with the U.S. Department of Energy. The United States Government retains and the publisher, by accepting the article for publication, acknowledges that the United States Government retains a non-exclusive, paid-up, irrevocable, world-wide license to publish or reproduce the published form of this manuscript, or allow others to do so, for United States Government purposes. The Department of Energy will provide public access to these results of federally sponsored research in accordance with the DOE Public Access Plan (http://energy.gov/downloads/doe-public-access-plan).

REFERENCES

1. B. D. Iverson, T. M. Conboy, J. J. Pasch, A. M. Kruizenga, Applied Energy, **111**, 957-970 (2013).
2. P. D. Myers Jr. and D. Y. Goswami, App. Thermal Eng. **109**, 889-900 (2016).
3. W. Ding, H. Shi, Y. Xiu, et al., Solar Energy Materials and Solar Cells **184**, 22-30 (2018).
4. H. Sun, J. Wang, Z. Lia, P. Zhang, X. Su, Solar Energy **171**, 320-329 (2018).
5. H. Susskind, F. B. Hill, L. Green, et al., Chemical Engineering Progress **56**, 57-63 (1960).
6. J. R. Keiser, J. H. DeVan and E. J. Lawrence, J. Nucl. Mater. **85-86**, 295-298 (1979) 295-298.
7. J. H. DeVan, J. Nucl. Mater. **85-86**, 249-256 (1979).
8. S. J. Pawel, Fusion Sci. Technol. **61**:1T, 369-374 (2012).
9. S. J. Pawel and K. A. Unocic, J. Nucl. Mater. **492**, 41-51 (2017).
10. B. A. Pint, J. W. McMurray, A. W. Willoughby, et al., Materials & Corrosion, 70 (2019) 1439-1449.
11. B. A. Pint, ORNL Report ORNL/SPR-2020/1940, Oak Ridge, TN (2020).
12. G.-S. Chen, I-W. Sun, K. D. Sienerth, et al., Journal Electrochemical Society, 140 (1993) 1523-1526.